

Unsupervised Discovery of Object Landmarks via Contrastive Learning

Zezhou Cheng Jong-Chyi Su Subhransu Maji
University of Massachusetts Amherst
{zezhoucheng, jcsu, smaji}@cs.umass.edu

Abstract

Given a collection of images, humans are able to discover landmarks of the depicted objects by modeling the shared geometric structure across instances. This idea of “*geometric equivariance*” has been widely used for unsupervised discovery of object landmark representations. In this paper, we develop a simple and effective approach based on contrastive learning of “*invariant*” representations. We show that when a deep network is trained to be invariant to geometric and photometric transformations, representations from its intermediate layers are highly predictive of object landmarks. Furthermore, by stacking representations across layers in a “*hypercolumn*” their effectiveness can be improved. Our approach is motivated by the phenomenon of the gradual emergence of invariance in the representation hierarchy of a deep network. We also present a unified view of existing equivariant and invariant representation learning approaches through the lens of contrastive learning, shedding light on the nature of invariances learned. Experiments on standard benchmarks for landmark discovery, as well as a challenging one we propose, show that the proposed approach surpasses prior state-of-the-art.

1 Introduction

Learning in the absence of labels is a challenge for existing machine learning and computer vision systems. Despite recent advances, the performance of unsupervised learning remains far below supervised learning, especially for few-shot image understanding tasks [16]. This paper considers the task of unsupervised learning of object landmarks from a collection of images. The goal is to learn representations from a large number of unlabeled images such that they allow accurate prediction of landmarks such as eyes and noses when provided with a few labeled examples.

One way of inferring structure is to reason about the global appearance in terms of disentangled factors such as geometry and texture. This is the basis of alignment based [24, 35] and generative modeling based approaches for landmark discovery [25, 26, 42, 52, 59]. An alternate is to learn a representation that geometrically deforms in the same way as the object, a property called *geometric equivariance* (Fig. 1a). However, a drawback of these approaches is that useful invariances may not be learned (*e.g.*, the raw pixel representation itself is equivariant). As a result, these approaches are not robust to nuisance factors such as background clutter, occlusion, and other inter-image variations, limiting their applicability.

A different line of work has proposed *contrastive learning* as an unsupervised objective [3, 4, 10, 18, 21–23, 37, 47, 53, 63]. This is commonly formulated as an objective defined over pairs of data. The goal is to learn a representation Φ that has higher similarity between an image \mathbf{x} and its transformation \mathbf{x}' than with a different one \mathbf{z} , *i.e.*, $\langle \Phi(\mathbf{x}), \Phi(\mathbf{x}') \rangle \gg \langle \Phi(\mathbf{x}), \Phi(\mathbf{z}) \rangle$, as illustrated in Fig. 1b. Transformations are obtained using a combination of geometric (*e.g.*, cropping and scaling)

Project webpage: https://people.cs.umass.edu/~zezhoucheng/contrastive_landmark

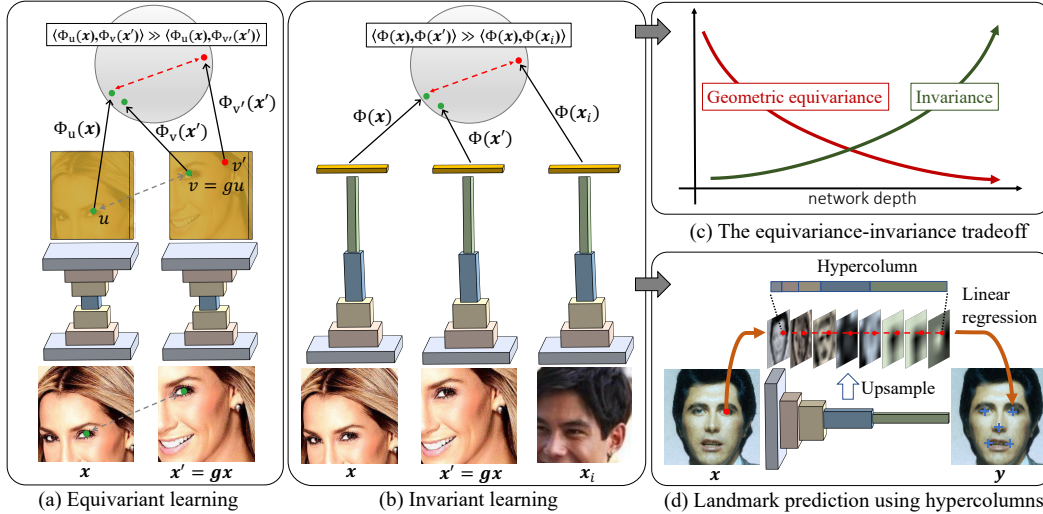


Figure 1: **Equivariant and invariant learning.** (a) Equivariant learning requires representations across locations to be invariant to a geometric transformation g while being distinctive across locations. (b) Invariant learning encourages the representations to be invariant to transformations while being distinctive across images. Thus both can be seen as instances of contrastive learning. (c) Invariance increases while geometric equivariance decreases with depth when a deep network is trained to be invariant to both geometric and photometric transformations. (d) A hypercolumn representation allows a linear model to select the right trade-off between desired invariances and equivariance.

and photometric (*e.g.*, color jittering and blurring) transformations, encouraging the representation to be *invariant* to these factors while being *distinctive* across images. Recent work [4, 21] has shown that contrastive learning is effective, even outperforming ImageNet [9] pretraining for a range of tasks and domains. However, in order to predict landmarks, a representation cannot be invariant to geometric transformations of an image. Moreover, their effectiveness in the few-shot setting has not been sufficiently studied. This paper asks the question: *are equivariant losses necessary for unsupervised landmark discovery?* In particular, do representations predictive of object landmarks automatically emerge in intermediate layers of a deep network trained to be invariant to image transformations, including geometric ones? While empirical evidence [15, 62] suggests the emergence of semantic parts in deep networks trained on supervised tasks, is it also the case for unsupervised learning?

This work aims to address these by presenting a unified view of the two approaches. We show that when a deep network is trained to be invariant to geometric and photometric transformations, its intermediate layer representations are highly predictive of landmarks (Fig. 1b). The emergence of invariance and the loss of geometric equivariance is gradual in the representation hierarchy, a phenomenon that has been studied empirically [29, 57] and theoretically [1, 48, 49] (Fig. 1c). As a result, its intermediate layer offers a better trade-off between desired invariances and equivariances for the landmark prediction task. This observation also motivates a *hypercolumn* representation [19], resulting in more accurate landmark predictions (Fig. 1d). We also observe that objectives used in equivariant learning can be seen as a contrastive loss between pixel representations at different locations within the *same image*, unlike invariant learning where the contrastive loss is applied *across images* (Fig. 1a vs 1b). This sheds light on the nature of invariances learned by these techniques.

To validate these claims, we present experiments using off-the-shelf Residual Networks [20] and the Momentum Contrast (MoCo) [21] learning on several benchmarks for landmark detection. We present a quantitative evaluation in a linear evaluation setting by varying the number of labeled examples. We also present a comparison by learning on a challenging dataset of birds from the iNaturalist dataset [50] and evaluating on the CUB dataset [51]. Our approach is simple, yet it offers consistent improvements over prior approaches [25, 44–46, 59]. While the hypercolumn representation leads to a larger embedding dimension, it comes at a modest cost as our approach outperforms the prior state-of-the-art [46], with as few as 50 annotated training examples on the AFLW benchmark [28] (Fig. 3). In fact, we observe that the hypercolumns of randomly initialized networks also offer a good generalization, suggesting that both the architecture and learning objective play an important role.

In summary, our contributions are as follows. We present a unified view of existing equivariant and the proposed invariant landmark representation learning approaches through the lens of contrastive learning — the former encourages intra-image invariance while the latter encourages inter-image invariance. We show that invariant representation learning using contrastive losses lead to more effective landmark representations than prior state-of-the-art on several benchmarks. The improvements are pronounced on a more challenging dataset we propose. We analyze and motivate the effectiveness of our approach by the phenomenon of the gradual emergence of invariance in the representation hierarchy and propose a hypercolumn representation which provides further benefits.

2 Related Work

Background. A representation $\Phi : \mathcal{X} \rightarrow \mathbb{R}^d$ is said to be equivariant (or covariant) with a transformation g for input $\mathbf{x} \in \mathcal{X}$ if there exists a map $M_g : \mathbb{R}^d \rightarrow \mathbb{R}^d$ such that: $\forall \mathbf{x} \in \mathcal{X} : \Phi(g\mathbf{x}) \approx M_g \Phi(\mathbf{x})$. In other words, the representation transforms in a predictable manner given the input transformation. For natural images, the transformations can be geometric (e.g., translation, scaling, and rotation), photometric (e.g., color changes), or more complex (e.g., occlusion, viewpoint or instance variations). Note that a sufficient condition for equivariance is when Φ is invertible since $M_g = \Phi^{-1} \circ g$. Invariance is a special case of equivariance when M_g is the identity function, i.e., $\phi(g\mathbf{x}) \approx \phi(\mathbf{x})$. There is a rich history in computer vision on the design of covariant (e.g., SIFT [33]), and invariant representations (e.g., HOG [8] and Bag-of-Visual-Words [43]).

Deep representations. Invariance and equivariance in deep network representations result from both the architecture (e.g., convolutions lead to translational equivariance, while pooling leads to translational invariance), and learning (e.g., invariance to categorical variations). Lenc and Vedaldi [29] showed that early-layer representations of deep networks trained on ImageNet are nearly equivariant as they can be “inverted” to recover the input, while later layers are more invariant. Similar observations have been made by visualizing these representations [34, 57]. The gradual emergence of invariance can also be theoretically understood in terms of a “information bottleneck” in the feed-forward hierarchy [1, 48, 49]. While equivariance to geometric transformations is relevant for landmark representations, the notion can be generalized to other transformation groups [7, 13].

Landmark discovery. Empirical evidence [38, 62] suggests that semantic parts emerge when deep networks are trained on supervised tasks. This has inspired architectures for image classification that encourage part-based reasoning, such as those based on texture representations [2, 6, 30] or spatial attention [12, 41, 55]. In contrast, our work shows that *parts also emerge when models are trained in an unsupervised manner*. When no labels are available, equivariance to geometric transformations provides a natural self-supervisory signal. The equivariance constraint requires $\Phi_u(\mathbf{x})$, the representation of \mathbf{x} at location u , to be invariant to the geometric transformation g of the image, i.e., $\forall \mathbf{x}, u : \Phi_{gu}(g\mathbf{x}) = \Phi_u(\mathbf{x})$ (Fig. 1a). This alone is not sufficient since both $\Phi_u(\mathbf{x}) = \mathbf{x}_u$ and $\Phi_u(\mathbf{x}) = \text{constant}$, satisfy this property. Constraints based on locality [44, 46] and diversity [45] have been proposed to avoid this pathology. Yet, inter-image invariance is not directly enforced. Another line of work is based on a generative modeling approach [25, 26, 32, 42, 52, 59]. These methods implicitly incorporate equivariant constraints by modeling objects as deformation (or flow) of a shape template together with appearance variation in a disentangled manner. In contrast, our work shows that learning representations invariant to both geometric and photometric transformations is an effective strategy. These invariances emerge at different rates in the representation hierarchy, and one can select the appropriate ones with a small amount of supervision for the downstream task.

Unsupervised learning. Recent work has shown that unsupervised objectives based on density modeling [3, 4, 10, 21, 23, 37, 47, 53], outperform unsupervised (or self-supervised) learning based on pretext tasks such as colorization [58], rotation prediction [14], jigsaw puzzle [36], and inpainting [39]. These contrastive learning objectives [18] are often expressed in terms of noise-contrastive estimation (NCE) [17] (or maximizing mutual information [23, 37]) between different views obtained by geometrically and photometrically transforming an image. The learned representations thus encode invariances to these transformations while preserving information relevant for downstream tasks. However, the effectiveness of unsupervised learning depends on how well these invariances relate to those desired for end tasks. Despite recent advances, existing methods for unsupervised learning significantly lack in comparison to their supervised counterparts in the few-shot setting [16]. Moreover, their effectiveness for landmark discovery has not been sufficiently studied in the litera-

ture.² In part, it is not clear why invariance to geometric transformations might be useful for landmark prediction since we require the representation to carry some spatial information about the image. Understanding these trade-offs and improving the effectiveness of contrastive learning for landmark prediction is one of the goals of the paper.

3 Method

Denote $\mathbf{x} \in \mathbb{R}^{H \times W \times 3}$ as an image of an object, and $u \in \Omega = \{0, \dots, H-1\} \times \{0, \dots, W-1\}$ as pixel coordinates. The target of unsupervised landmark discovery is to learn an encoder $\Phi_u(\mathbf{x}) : \Omega \rightarrow \mathbb{R}^C$ to generate representation at spatial location u of input \mathbf{x} which is predictive for object landmarks. We assume $C \gg 3$ aiming to learn a high-dimensional representation of landmarks. This is similar to [46] which learns a local descriptor for each landmark, and unlike those that represent them as a discrete set [61], or on a planar ($C = 2$) [45, 59] or spherical ($C = 3$) [44] coordinate system. In other words, the representation should be predictive of landmarks (measured using a linear regressor), without requiring compactness or topology in the embedding space.

We describe commonly used equivariance constraints for unsupervised landmark discovery [44–46], followed by models based on invariant learning [21, 37]. We then present a unified view of the two approaches motivating our approach, which is to simply train a deep network to be invariant to all transformations and use features from intermediate layers as the landmark representation.

3.1 Equivariant and invariant representation learning

Equivariant learning. The equivariance constraint requires $\Phi_u(\mathbf{x})$, the representation of \mathbf{x} at location u , to be invariant to the geometric deformation of the image (Fig. 1a). Given a geometric warping function $g : \Omega \rightarrow \Omega$, the representation of \mathbf{x} at u should be same as the representation of the transformed image $\mathbf{x}' = g\mathbf{x}$ at $v = gu$, that is, $\forall \mathbf{x}, u \in \Omega : \Phi_v(\mathbf{x}') = \Phi_u(\mathbf{x})$. This constraint can be captured by the loss:

$$\mathcal{L}_{equi} = \frac{1}{|\Omega|} \sum_{u \in \Omega} \|\Phi_u(\mathbf{x}) - \Phi_v(\mathbf{x}')\|^2. \quad (1)$$

A diversity (or locality) constraint is necessary to encourage the representation to be distinctive across locations. For example, [44] proposed the following:

$$\mathcal{L}_{div} = \frac{1}{|\Omega|} \sum_{u \in \Omega} \|gu - \underset{v}{\operatorname{argmax}} \langle \Phi_u(\mathbf{x}), \Phi_v(\mathbf{x}') \rangle\|^2, \quad (2)$$

which they replace by a probabilistic version that combines both the losses as:

$$\mathcal{L} = \frac{1}{|\Omega|^2} \sum_{u \in \Omega} \sum_{v \in \Omega} \|gu - v\| p(v|u; \Phi, \mathbf{x}, \mathbf{x}'). \quad (3)$$

Here $p(v|u; \Phi, \mathbf{x}, \mathbf{x}')$ is the probability of pixel u in image \mathbf{x} matching v in image \mathbf{x}' with Φ as the encoder shared by \mathbf{x} and \mathbf{x}' computed as below, and $\tau \in \mathbb{R}^+$ is a scale parameter:

$$p(v|u; \Phi, \mathbf{x}, \mathbf{x}') = \frac{\exp(\langle \Phi_u(\mathbf{x}), \Phi_v(\mathbf{x}') \rangle / \tau)}{\sum_{t \in \Omega} \exp(\langle \Phi_u(\mathbf{x}), \Phi_t(\mathbf{x}') \rangle / \tau)}. \quad (4)$$

Invariant learning. Contrastive representation learning is based on similarity over pairs of inputs (Fig. 1b). Given an image \mathbf{x} and its transformation \mathbf{x}' as well as other images $\mathbf{x}_i, i \in \{1, 2, \dots, N\}$, the InfoNCE [37] loss minimizes:

$$\mathcal{L}_{NCE} = -\log \frac{\exp(\langle \Phi(\mathbf{x}), \Phi(\mathbf{x}') \rangle)}{\sum_{i=1}^N \exp(\langle \Phi(\mathbf{x}), \Phi(\mathbf{x}_i) \rangle)}. \quad (5)$$

The objective encourages representations to be invariant to transformations while being distinctive across images. To address the computational bottleneck in evaluating the denominator, Momentum

²Note that MoCo [21] was evaluated on pose estimation, however their method was trained with 150K labeled examples and the entire network was fine-tuned.

Contrast (MoCo) [21] replaces the loss over negative examples using a dictionary queue and updates the parameters based on momentum.

Transformations. The space of transformations used to generate image pairs $(\mathbf{x}, \mathbf{x}')$ plays an important role in learning. A common approach is to apply a combination of *geometric transformations*, such as cropping, resizing, and thin-plate spline warps, as well as *photometric transformations*, such as color jittering, JPEG noise, and PCA color augmentation. However, transformations can also denote different color channels of an image or different modalities such as depth and color [47].

Hypercolumns. A deep network of n layers (or blocks³) can be written as $\Phi(\mathbf{x}) = \Phi^{(n)} \circ \Phi^{(n-1)} \circ \dots \circ \Phi^{(1)}(\mathbf{x})$. A representation $\Phi(\mathbf{x})$ of size $H' \times W' \times C$ can be spatially interpolated to the input size $H \times W \times C$ to produce a pixel representation $\Phi_u(\mathbf{x}) \in \mathbb{R}^C$. The hypercolumn representation of layers k_1, k_2, \dots, k_n is obtained by concatenating the interpolated features from the corresponding layers, that is, $\Phi_u(\mathbf{x}) = \Phi_u^{(k_1)}(\mathbf{x}) \oplus \Phi_u^{(k_2)}(\mathbf{x}) \oplus \dots \oplus \Phi_u^{(k_n)}(\mathbf{x})$.

Our approach. Given a large unlabeled dataset, we first train invariant representations using contrastive learning [21] with a combination of geometric and photometric transformations applied to images to generate pairs. We then extract single or hypercolumn representation from intermediate layers to represent landmarks (Fig. 1b and Fig. 1d).

3.2 A unified view of the two approaches

Commonalities and differences. Equivariance is necessary but not sufficient for an effective landmark representation. It also needs to be distinctive or invariant to nuisance factors. This is enforced in the equivariance objective (Eq. 3) as a contrastive term over locations within the same image, as the loss is minimized when $p(v|u; \Phi, \mathbf{x}, \mathbf{x}')$ is maximized at $v = gu$. This encourages intra-image invariance, unlike the objective of contrastive learning (Eq. 5), which encourages inter-image invariance. However, a single image may contain enough variety to guarantee some invariance. This is supported by its empirical performance and recent work showing that representation learning is possible even from a single image [56]. However, our experiments suggest that on challenging datasets, with objects in clutter, occlusion, and wider pose variation, inter-image invariance can be more effective.

Why do landmarks emerge during invariant learning? For this, we point to the phenomenon of the gradual emergence of invariance in the representation hierarchy [1, 29, 48, 49]. In particular, equivariance to geometric transformations reduces with depth due to pooling operations, while invariance to nuisance factors increases with depth (Fig. 1c). Thus, picking an intermediate layer in the representation hierarchy may offer the desired trade-off between the geometric equivariance and invariances for predicting landmarks. Our experiments support this, and we find that it is possible to select the right layer with just a few labeled examples from the downstream task. The scheme can be further improved by stacking representations across layers in a hypercolumn (Sec. 4).

Is there any advantage of one approach over the other? Our experiments show that for a deep network of the same size, invariant representation learning can be just as effective (Tab. 1). However, invariant learning is conceptually simpler and scales better than equivariance approaches, as the latter maintains high-resolution feature maps across the hierarchy. Using a deeper network (*e.g.*, ResNet50 vs. ResNet18) results in consistent improvements, outperforming DVE [46] on four out of five datasets, as shown in Tab. 1. A drawback of our approach is that the representation is not directly interpretable or compact, which results in lower performance in the extreme few-shot case. However, as seen in Fig. 3a, the advantage disappears with as few as 50 training examples on the AFLW benchmark [28]. Moreover, invariant learning makes better use of data achieving the same performance with half the unlabeled examples, as seen in Fig. 3c. We describe these experiments in detail in the next section.

4 Experiments

We first outline the datasets and implementation details of the proposed method (Sec. 4.1). We then evaluate our model and provide comparisons to the existing methods qualitatively and quantitatively on the landmark detection benchmarks, followed by a thorough ablation study (Sec. 4.2).

³Due to skip-connections, we cannot decompose the encoding over layers, but can across blocks.

4.1 Benchmarks and implementation details

Human faces. We first compare the proposed model with prior art on the existing human face landmark detection benchmarks. Following DVE [46], we train our model on CelebA dataset [31] and evaluate on MAFL [61], AFLW [28], and 300W [40]. The overlapping images with MAFL are excluded from CelebA. MAFL comprises 19,000 training images and 1000 testing images with annotations on 5 face landmarks. Two versions of AFLW are used: AFLW_M that contains 10,122 training images and 2995 testing images, which are crops from MTFI [60]; AFLW_R which contains tighter crops of face images with 10,122 for training and 2991 for testing. 300W provides 68 annotated face landmarks with 3148 training images and 689 testing images. We apply the same image pre-processing procedures as in DVE, the current state-of-the-art, for a direct comparison.

Birds. We collect a challenging dataset of birds where objects appear in clutter, occlusion, and exhibit wider pose variation. We randomly select 100K images of birds from the iNaturalist 2017 dataset [50] under the “Aves” class to train unsupervised representations. For the performance on the few-shot setting, we collect a subset of CUB dataset [51] containing 35 species of *Passeroidea* superfamily, each annotated with 15 landmarks⁴. We sample at most 60 images per class which results in 1241 images as our training set, 382 as validation set, and 383 as testing set (see Appendix E for details).

Evaluation. We use landmark regression as the end task for evaluation. Following [44, 46], we train a linear regressor to map the representations to landmark annotations, keeping the representation frozen. The landmark regressor is a linear regressor per target landmark. Each regressor consists of 50 filters of size $1 \times 1 \times C$ on top of a C -dimensional representation to generate 50 intermediate heatmaps, which are then converted to spatial coordinates by `soft-argmax` operation. These 50 coordinates are finally converted to the target landmark by a linear layer (see Appendix A for details). We report errors in the percentage of inter-ocular distance on face benchmarks and the percentage of correct keypoints (PCK) on CUB. A prediction is considered correct according to the PCK metric if its distance to the ground-truth is within 5% of the longer side of the image. The occluded landmarks are ignored during evaluation. We did not find fine-tuning to be uniformly beneficial but include a comparison in Appendix A.

Implementation details. We use MoCo [21] to train our models on CelebA or iNat Aves for 800 epochs with a batch size of 256 and a dictionary size of 4096. ResNet18 or ResNet50 [20] are used as our backbone. We extract hypercolumns [19] per pixel by stacking activations from the second (`conv2_x`) to the last convolutional block (`conv5_x`). We resize the feature maps from the selected convolutional blocks to the same spatial size as DVE [46] (*i.e.* 48×48). We also follow DVE (with Hourglass network) to resize the input image to 136×136 then center-crop the image to 96×96 for face datasets. Images are resized to 96×96 without any cropping on bird dataset. For a comparison with DVE on CUB dataset we used their publicly available implementation.

4.2 Results on landmark detection and ablation studies

Quantitative results. Tab. 1 presents a quantitative evaluation of multiple benchmarks. On faces, the proposed model with ResNet18 significantly outperforms several prior works [44, 45] and DVE with SmallNet. Our model with a ResNet50 achieves state-of-the-art results on all benchmarks except for 300W. On iNat Aves \rightarrow CUB, the approach outperforms prior state-of-the-art [46] by a large margin, suggesting improved invariance to nuisance factors.

Qualitative results. Fig. 2 shows the qualitative results of landmark regression on human faces and birds. We notice that both DVE and our model are able to localize the foreground object accurately. However, our model localizes many keypoints better (*e.g.*, on the tails of the birds) and is more robust to the background clutter (*e.g.*, the last column of Fig. 2b).

Limited annotations. Fig. 3a and 3b compare our model with DVE [46] using a limited number of annotations on AFLW_M and CUB dataset respectively. Our performance is better as soon as a few training examples are available (*e.g.*, 50 on AFLW_M and 250 on CUB). This can be attributed to the higher dimensional embedding of the hypercolumn representation. The scheme can be improved by using a single-layer representation as shown in the yellow line. Note that all unsupervised learning models (including DVE and our model) outperform the randomly initialized baseline on both human face and bird datasets. We provide the numbers corresponding to Fig. 3 in Appendix F.

⁴This is the biggest Aves taxa in iNaturalist.

Table 1: **Results on landmark detection.** Comparison on face benchmarks, including MAFL, AFLW_M, AFLW_R, and 300W, and CUB dataset. We report the error in the percentage of inter-ocular distance on human face dataset (*lower is better*), and the percentage of correct keypoints (PCK) on CUB dataset (*higher is better*). Our approach outperforms prior work on four out of five benchmarks. Superscripts in the last row denote the (%) error reduction over DVE Hourglass [46].

Method	# Params. Millions	Unsuper.	MAFL	AFLW _M	AFLW _R	300W	CUB PCK ↑
Inter-ocular Distance (%) ↓							
TCDCN [61]	–	×	7.95	7.65	–	5.54	–
RAR [54]	–	×	–	7.23	–	4.94	–
MTCNN [60]	–	×	5.39	6.90	–	–	–
Wing Loss [11]	–	×	–	–	–	4.04	–
Generative modeling based							
Structural Repr. [59]	–	✓	3.15	–	6.58	–	–
FAB-Net [52]	–	✓	3.44	–	–	5.71	–
Deforming AE [42]	–	✓	5.45	–	–	–	–
ImGen. [25]	–	✓	2.54	–	6.31	–	–
ImGen.++ [26]	–	✓	–	–	–	5.12	–
Equivariance based							
Sparse [45]	–	✓	6.67	10.53	–	7.97	–
Dense 3D [44]	–	✓	4.02	10.99	10.14	8.23	–
DVE SmallNet [46]	0.35	✓	3.42	8.60	7.79	5.75	–
DVE Hourglass [46]	12.61	✓	2.86	7.53	6.54	4.65	61.91
Invariance based							
Ours (ResNet18)	11.24	✓	2.57	8.59	7.38	5.78	62.24
Ours (ResNet50)	23.77	✓	2.44 ^{14.7}	6.99 ^{7.2}	6.27 ^{4.1}	5.22 ^{-12.3}	68.63 ^{17.6}

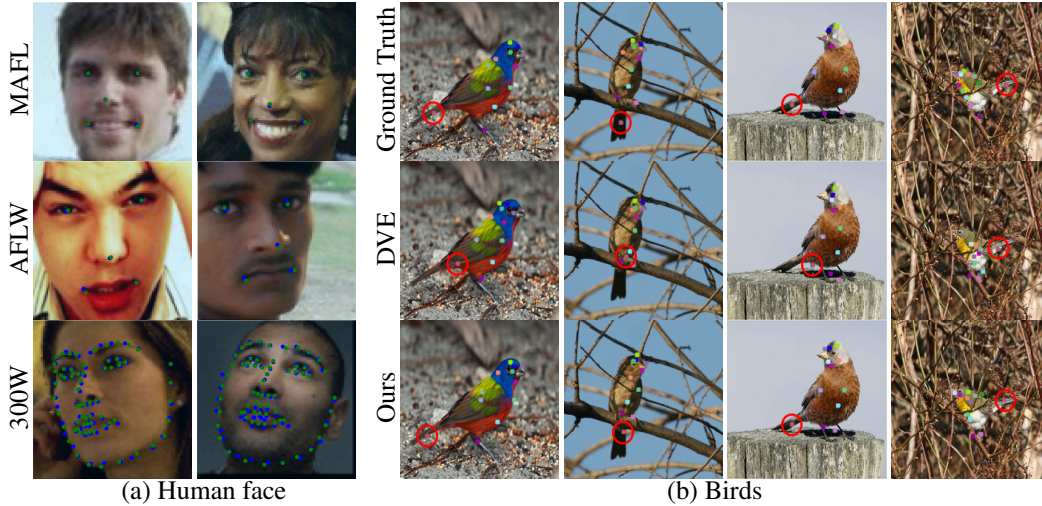


Figure 2: **Detected landmarks.** on (a) faces (*blue*: predictions, *green*: ground truth) and (b) CUB. Notice that our method localizes tails of birds (circled) much better. *Zoom in for details.*

Limited unlabeled data. Fig. 3c shows that our model matches the performance of DVE on AFLW_M using only 40% of the images on the CelebA dataset.

Hypercolumns. Tab. 2 compares the performance of using individual layer and hypercolumn representations. The activation from the fourth convolutional block consistently outperforms those from the other layers. For an input of size 96×96 , the spatial dimension of the representation is 48×48 at Layer #1 and 3×3 at Layer #5, reducing by a factor of two at each successive layer. Thus, while the representation loses geometric equivariance with depth, contrastive learning encourages invariance, resulting in Layer #4 with the optimal trade-off for this task. While the best layer can be selected with some labeled validation data, the hypercolumn representation provides further benefits everywhere except the very small data regime (Tab. 2 and Fig. 3a).

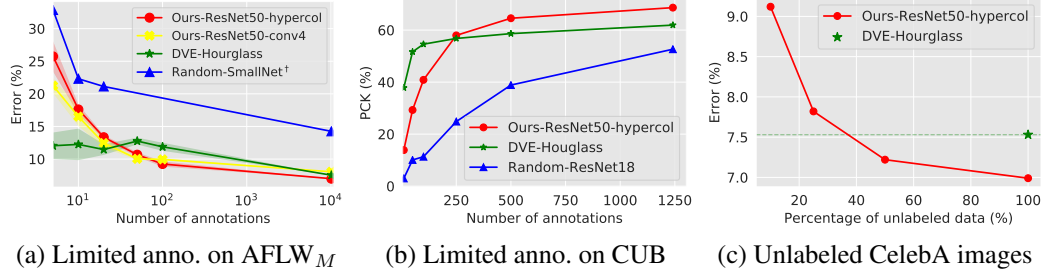


Figure 3: **The effect of dataset size.** (a) A comparison of our model with DVE [46] by varying the number of annotations for landmark regression on AFLW_M dataset. Random-SmallNet[†]: is a randomly initialized “small network” taken from [46]. Ours-ResNet50: are based on hypercolumn or forth-layer representations trained using contrastive learning. (b) Similar results on CUB dataset. Random-ResNet18: is trained from scratch on the CUB dataset. (c) Results of landmark regression on AFLW_M using different numbers of *unlabeled* images from CelebA for training.

Table 2: **Landmark detection using single layer and hypercolumn representations.** The error is reported in the percentage of inter-ocular distance using linear regression over individual layers (left) and combinations (right), with a ResNet50. The embedding dimension for each is shown in parenthesis. Layer #4 performs the best across datasets, while hypercolumns offer an improvement.

Dataset	Single layer					Hypercolumn			
	#1 (64)	#2 (256)	#3 (512)	#4 (1024)	#5 (2048)	#4 - #5 (3072)	#3 - #5 (3584)	#2 - #5 (3840)	#1 - #5 (3904)
MAFL	5.77	4.58	3.03	2.73	3.66	2.73	2.65	2.44	2.51
AFLW _M	24.20	21.34	11.95	8.83	11.55	8.14	8.31	6.99	7.40
AFLW _R	16.27	14.15	9.66	7.37	8.83	6.95	6.24	6.27	6.34
300W	16.45	13.08	7.66	6.01	7.70	5.68	5.28	5.22	5.21

Effectiveness of unsupervised learning. Tab. 3 compares representations using the linear evaluation setting for randomly initialized, ImageNet pretrained, and contrastively learned networks using a hypercolumn representation. Contrastive learning provides significant improvements over ImageNet pretrained models, which is less surprising since the domain of ImageNet images is quite different from faces. Interestingly, random networks have competitive performances with respect to some prior work in Tab. 1. For example, [44] achieve 4.02% on MAFL, while a randomly initialized ResNet18 with hypercolumns achieves 4.00%.

Table 3: **Effectiveness of unsupervised learning.** Error using randomly initialized, ImageNet pretrained, and contrastively trained ResNet18 (left) and ResNet50 (right) for landmark detection. Frozen hypercolumn representations with a linear regression were used for all methods.

ResNet18					ResNet50				
Supervision	MAFL	AFLW _M	AFLW _R	300W	Supervision	MAFL	AFLW _M	AFLW _R	300W
Random	4.00	14.20	10.11	9.88	Random	4.72	16.74	11.23	11.70
ImageNet	2.85	8.76	7.03	6.66	ImageNet	2.98	8.88	7.34	6.88
Contrastive	2.57	8.59	7.38	5.78	Contrastive	2.44	6.99	6.27	5.22

5 Conclusion

We show that landmark representations extracted from intermediate layers of a deep network trained to be invariant outperform existing unsupervised landmark representation learning approaches. We also show that several equivariant learning approaches can be viewed through the lens of contrastive learning — they learn intra-image invariances which result in weaker generalization than inter-image invariances on a more challenging benchmark we propose. However, the two approaches are complementary and may be combined for further benefits.

Broader Impact

This work falls in the general category of unsupervised learning which aims to discover structure from unlabeled data. In particular this work reduces annotation costs associated with training object landmark detectors, potentially allowing novel applications in domains where there are no existing large-scale labeled datasets. On the other hand, without expert supervision, the methods may inherit and amplify the biases from data causing poor performance on downstream applications.

Acknowledgments and Disclosure of Funding

The project is supported in part by Grants #1661259 and #1749833 from the National Science Foundation of United States. Our experiments were performed on the University of Massachusetts, Amherst GPU cluster obtained under the Collaborative Fund managed by the Massachusetts Technology Collaborative. We would also like to thank Erik Learned-Miller, Dan Sheldon and Rui Wang for discussion and feedback on the draft.

References

- [1] Alessandro Achille and Stefano Soatto. Emergence of invariance and disentanglement in deep representations. *The Journal of Machine Learning Research*, 19(1):1947–1980, 2018. 2, 3, 5
- [2] Relja Arandjelovic, Petr Gronat, Akihiko Torii, Tomas Pajdla, and Josef Sivic. Netvlad: Cnn architecture for weakly supervised place recognition. In *Proceedings of the IEEE conference on computer vision and pattern recognition*, pages 5297–5307, 2016. 3
- [3] Philip Bachman, R Devon Hjelm, and William Buchwalter. Learning representations by maximizing mutual information across views. In *Advances in Neural Information Processing Systems*, pages 15509–15519, 2019. 1, 3
- [4] Ting Chen, Simon Kornblith, Mohammad Norouzi, and Geoffrey Hinton. A simple framework for contrastive learning of visual representations. *arXiv preprint arXiv:2002.05709*, 2020. 1, 2, 3
- [5] Xinlei Chen, Haoqi Fan, Ross Girshick, and Kaiming He. Improved baselines with momentum contrastive learning. *arXiv preprint arXiv:2003.04297*, 2020. 13
- [6] Mircea Cimpoi, Subhransu Maji, and Andrea Vedaldi. Deep filter banks for texture recognition and segmentation. In *Proceedings of the IEEE conference on computer vision and pattern recognition*, pages 3828–3836, 2015. 3
- [7] Taco Cohen and Max Welling. Group equivariant convolutional networks. In *International conference on machine learning*, pages 2990–2999, 2016. 3
- [8] Navneet Dalal and Bill Triggs. Histograms of oriented gradients for human detection. In *Proceedings of the IEEE conference on computer vision and pattern recognition*, volume 1, pages 886–893. IEEE, 2005. 3
- [9] Jia Deng, Wei Dong, Richard Socher, Li-Jia Li, Kai Li, and Li Fei-Fei. Imagenet: A large-scale hierarchical image database. In *2009 IEEE conference on computer vision and pattern recognition*, pages 248–255. Ieee, 2009. 2
- [10] Alexey Dosovitskiy, Jost Tobias Springenberg, Martin Riedmiller, and Thomas Brox. Discriminative unsupervised feature learning with convolutional neural networks. In *Advances in Neural Information Processing Systems (NeurIPS)*, 2014. 1, 3
- [11] Zhen-Hua Feng, Josef Kittler, Muhammad Awais, Patrik Huber, and Xiao-Jun Wu. Wing loss for robust facial landmark localisation with convolutional neural networks. In *Proceedings of the IEEE Conference on Computer Vision and Pattern Recognition*, pages 2235–2245, 2018. 7
- [12] Jianlong Fu, Heliang Zheng, and Tao Mei. Look closer to see better: Recurrent attention convolutional neural network for fine-grained image recognition. In *Proceedings of the IEEE conference on computer vision and pattern recognition*, pages 4438–4446, 2017. 3

- [13] Robert Gens and Pedro M Domingos. Deep symmetry networks. In *Advances in neural information processing systems*, pages 2537–2545, 2014. 3
- [14] Spyros Gidaris, Praveer Singh, and Nikos Komodakis. Unsupervised representation learning by predicting image rotations. In *International Conference on Learning Representations (ICLR)*, 2018. 3
- [15] Abel Gonzalez-Garcia, Davide Modolo, and Vittorio Ferrari. Do semantic parts emerge in convolutional neural networks? *International Journal of Computer Vision*, 126(5):476–494, 2018. 2
- [16] Priya Goyal, Dhruv Mahajan, Abhinav Gupta, and Ishan Misra. Scaling and benchmarking self-supervised visual representation learning. In *International Conference on Computer Vision (ICCV)*, 2019. 1, 3
- [17] Michael Gutmann and Aapo Hyvärinen. Noise-contrastive estimation: A new estimation principle for unnormalized statistical models. In *Proceedings of the Thirteenth International Conference on Artificial Intelligence and Statistics*, pages 297–304, 2010. 3
- [18] Raia Hadsell, Sumit Chopra, and Yann LeCun. Dimensionality reduction by learning an invariant mapping. In *Proceedings of the IEEE conference on computer vision and pattern recognition*, volume 2, pages 1735–1742. IEEE, 2006. 1, 3
- [19] Bharath Hariharan, Pablo Arbeláez, Ross Girshick, and Jitendra Malik. Hypercolumns for object segmentation and fine-grained localization. In *Proceedings of the IEEE conference on computer vision and pattern recognition*, pages 447–456, 2015. 2, 6
- [20] Kaiming He, Xiangyu Zhang, Shaoqing Ren, and Jian Sun. Deep residual learning for image recognition. In *Proceedings of the IEEE conference on computer vision and pattern recognition*, pages 770–778, 2016. 2, 6
- [21] Kaiming He, Haoqi Fan, Yuxin Wu, Saining Xie, and Ross Girshick. Momentum contrast for unsupervised visual representation learning. *arXiv preprint arXiv:1911.05722*, 2019. 1, 2, 3, 4, 5, 6, 13
- [22] Olivier J Hénaff, Aravind Srinivas, Jeffrey De Fauw, Ali Razavi, Carl Doersch, SM Eslami, and Aaron van den Oord. Data-efficient image recognition with contrastive predictive coding. *arXiv preprint arXiv:1905.09272*, 2019.
- [23] R Devon Hjelm, Alex Fedorov, Samuel Lavoie-Marchildon, Karan Grewal, Phil Bachman, Adam Trischler, and Yoshua Bengio. Learning deep representations by mutual information estimation and maximization. In *International Conference on Learning Representations (ICLR)*, 2019. 1, 3
- [24] Gary Huang, Marwan Mattar, Honglak Lee, and Erik G Learned-Miller. Learning to align from scratch. In *Advances in neural information processing systems*, pages 764–772, 2012. 1
- [25] Tomas Jakab, Ankush Gupta, Hakan Bilen, and Andrea Vedaldi. Unsupervised learning of object landmarks through conditional image generation. In *Advances in Neural Information Processing Systems*, pages 4016–4027, 2018. 1, 2, 3, 7
- [26] Tomas Jakab, Ankush Gupta, Hakan Bilen, and Andrea Vedaldi. Self-supervised learning of interpretable keypoints from unlabelled videos. In *Proceedings of the IEEE Conference on Computer Vision and Pattern Recognition*, 2020. 1, 3, 7
- [27] Diederik P Kingma and Jimmy Ba. Adam: A method for stochastic optimization. *arXiv preprint arXiv:1412.6980*, 2014. 14
- [28] Martin Koestinger, Paul Wohlhart, Peter M Roth, and Horst Bischof. Annotated facial landmarks in the wild: A large-scale, real-world database for facial landmark localization. In *2011 IEEE international conference on computer vision workshops (ICCV workshops)*, pages 2144–2151. IEEE, 2011. 2, 5, 6

- [29] Karel Lenc and Andrea Vedaldi. Understanding image representations by measuring their equivariance and equivalence. In *Proceedings of the IEEE conference on computer vision and pattern recognition*, pages 991–999, 2015. 2, 3, 5
- [30] Tsung-Yu Lin, Aruni RoyChowdhury, and Subhransu Maji. Bilinear cnn models for fine-grained visual recognition. In *Proceedings of the IEEE international conference on computer vision*, pages 1449–1457, 2015. 3
- [31] Ziwei Liu, Ping Luo, Xiaogang Wang, and Xiaoou Tang. Deep learning face attributes in the wild. In *Proceedings of the IEEE international conference on computer vision*, pages 3730–3738, 2015. 6
- [32] Dominik Lorenz, Leonard Bereska, Timo Milbich, and Bjorn Ommer. Unsupervised part-based disentangling of object shape and appearance. In *Proceedings of the IEEE Conference on Computer Vision and Pattern Recognition*, pages 10955–10964, 2019. 3
- [33] David G Lowe. Distinctive image features from scale-invariant keypoints. *International journal of computer vision*, 60(2):91–110, 2004. 3
- [34] Aravindh Mahendran and Andrea Vedaldi. Visualizing deep convolutional neural networks using natural pre-images. *International Journal of Computer Vision*, 120(3):233–255, 2016. 3
- [35] Erik G Miller, Nicholas E Matsakis, and Paul A Viola. Learning from one example through shared densities on transforms. In *Proceedings IEEE Conference on Computer Vision and Pattern Recognition.*, volume 1, pages 464–471. IEEE, 2000. 1
- [36] Mehdi Noroozi and Paolo Favaro. Unsupervised learning of visual representations by solving jigsaw puzzles. In *European Conference on Computer Vision (ECCV)*, 2016. 3
- [37] Aaron van den Oord, Yazhe Li, and Oriol Vinyals. Representation learning with contrastive predictive coding. *arXiv preprint arXiv:1807.03748*, 2018. 1, 3, 4
- [38] Maxime Oquab, Léon Bottou, Ivan Laptev, and Josef Sivic. Is object localization for free?-weakly-supervised learning with convolutional neural networks. In *Proceedings of the IEEE conference on computer vision and pattern recognition*, pages 685–694, 2015. 3
- [39] Deepak Pathak, Philipp Krahenbuhl, Jeff Donahue, Trevor Darrell, and Alexei A Efros. Context encoders: Feature learning by inpainting. In *Proceedings of the IEEE Conference on Computer Vision and Pattern Recognition (CVPR)*, 2016. 3
- [40] Christos Sagonas, Georgios Tzimiropoulos, Stefanos Zafeiriou, and Maja Pantic. 300 faces in-the-wild challenge: The first facial landmark localization challenge. In *Proceedings of the IEEE International Conference on Computer Vision Workshops*, pages 397–403, 2013. 6
- [41] Pierre Sermanet, Andrea Frome, and Esteban Real. Attention for fine-grained categorization. *arXiv preprint arXiv:1412.7054*, 2014. 3
- [42] Zhixin Shu, Mihir Sahasrabudhe, Riza Alp Guler, Dimitris Samaras, Nikos Paragios, and Iasonas Kokkinos. Deforming autoencoders: Unsupervised disentangling of shape and appearance. In *Proceedings of the European Conference on Computer Vision*, pages 650–665, 2018. 1, 3, 7
- [43] Josef Sivic and Andrew Zisserman. Video google: A text retrieval approach to object matching in videos. In *International Conference on Computer Vision (ICCV)*, page 1470. IEEE, 2003. 3
- [44] James Thewlis, Hakan Bilen, and Andrea Vedaldi. Unsupervised learning of object frames by dense equivariant image labelling. In *Advances in neural information processing systems*, pages 844–855, 2017. 2, 3, 4, 6, 7, 8
- [45] James Thewlis, Hakan Bilen, and Andrea Vedaldi. Unsupervised learning of object landmarks by factorized spatial embeddings. In *Proceedings of the IEEE International Conference on Computer Vision*, pages 5916–5925, 2017. 3, 4, 6, 7
- [46] James Thewlis, Samuel Albanie, Hakan Bilen, and Andrea Vedaldi. Unsupervised learning of landmarks by descriptor vector exchange. In *Proceedings of the IEEE International Conference on Computer Vision*, pages 6361–6371, 2019. 2, 3, 4, 5, 6, 7, 8, 13, 14, 16

- [47] Yonglong Tian, Dilip Krishnan, and Phillip Isola. Contrastive multiview coding. *arXiv:1906.05849*, 2019. 1, 3, 5, 14
- [48] Naftali Tishby and Noga Zaslavsky. Deep learning and the information bottleneck principle. In *2015 IEEE Information Theory Workshop (ITW)*, pages 1–5. IEEE, 2015. 2, 3, 5
- [49] Naftali Tishby, Fernando C Pereira, and William Bialek. The information bottleneck method. *arXiv preprint physics/0004057*, 2000. 2, 3, 5
- [50] Grant Van Horn, Oisin Mac Aodha, Yang Song, Yin Cui, Chen Sun, Alex Shepard, Hartwig Adam, Pietro Perona, and Serge Belongie. The iNaturalist species classification and detection dataset. In *Proceedings of the IEEE Conference on Computer Vision and Pattern Recognition (CVPR)*, 2018. 2, 6, 14
- [51] C. Wah, S. Branson, P. Welinder, P. Perona, and S. Belongie. The Caltech-UCSD Birds-200-2011 Dataset. Technical Report CNS-TR-2011-001, California Institute of Technology, 2011. 2, 6
- [52] Olivia Wiles, A Koepke, and Andrew Zisserman. Self-supervised learning of a facial attribute embedding from video. In *British Machine Vision Conference*, 2018. 1, 3, 7
- [53] Zhirong Wu, Yuanjun Xiong, Stella Yu, and Dahua Lin. Unsupervised feature learning via non-parametric instance discrimination. In *Proceedings of the IEEE Conference on Computer Vision and Pattern Recognition (CVPR)*, 2018. 1, 3
- [54] Shengtao Xiao, Jiashi Feng, Junliang Xing, Hanjiang Lai, Shuicheng Yan, and Ashraf Kassim. Robust facial landmark detection via recurrent attentive-refinement networks. In *European conference on computer vision*, pages 57–72. Springer, 2016. 7
- [55] Tianjun Xiao, Yichong Xu, Kuiyuan Yang, Jiaying Zhang, Yuxin Peng, and Zheng Zhang. The application of two-level attention models in deep convolutional neural network for fine-grained image classification. In *Proceedings of the IEEE conference on computer vision and pattern recognition*, pages 842–850, 2015. 3
- [56] Asano YM., Rupprecht C., and Vedaldi A. A critical analysis of self-supervision, or what we can learn from a single image. In *International Conference on Learning Representations (ICLR)*, 2020. 5
- [57] Matthew D Zeiler and Rob Fergus. Visualizing and understanding convolutional networks. In *European conference on computer vision*, pages 818–833. Springer, 2014. 2, 3
- [58] Richard Zhang, Phillip Isola, and Alexei A Efros. Colorful image colorization. In *European Conference on Computer Vision (ECCV)*, 2016. 3
- [59] Yuting Zhang, Yijie Guo, Yixin Jin, Yijun Luo, Zhiyuan He, and Honglak Lee. Unsupervised discovery of object landmarks as structural representations. In *Proceedings of the IEEE Conference on Computer Vision and Pattern Recognition*, pages 2694–2703, 2018. 1, 2, 3, 4, 7
- [60] Zhanpeng Zhang, Ping Luo, Chen Change Loy, and Xiaoou Tang. Facial landmark detection by deep multi-task learning. In *European conference on computer vision*, pages 94–108. Springer, 2014. 6, 7
- [61] Zhanpeng Zhang, Ping Luo, Chen Change Loy, and Xiaoou Tang. Learning deep representation for face alignment with auxiliary attributes. *IEEE transactions on pattern analysis and machine intelligence*, 38(5):918–930, 2015. 4, 6, 7
- [62] Bolei Zhou, Aditya Khosla, Agata Lapedriza, Aude Oliva, and Antonio Torralba. Learning deep features for discriminative localization. In *Proceedings of the IEEE conference on computer vision and pattern recognition*, pages 2921–2929, 2016. 2, 3
- [63] Chengxu Zhuang, Alex Lin Zhai, and Daniel Yamins. Local aggregation for unsupervised learning of visual embeddings. In *Proceedings of the IEEE International Conference on Computer Vision*, pages 6002–6012, 2019. 1

Appendix

A Fine-tuning the network

Tab. 4 presents the effect of fine-tuning all layers of our model end-to-end on multiple face landmark regression benchmarks. In this experiment, we use the output of the forth convolutional block of ResNet50 as the representation (which is the optimal single layer representation). We did *not* find fine-tuning to be uniformly beneficial — fine-tuning is worse than training the linear regressor only on MAFL dataset, while it is better on AFLW dataset. We speculate that this is because of the domain gap between the two training sets of unsupervised learning (contrastive learning) and supervised learning (linear regressor) and small training set sizes. CelebA and AFLW has larger domain gap than CelebA and MAFL, which is also noticed in DVE [46]. DVE approach fine-tuned the feature extractor on AFLW in the stage of unsupervised representation learning, however, we did not observe improvement from such unsupervised fine-tuning method in our experiments.

Table 4: **The effect of fine-tuning for landmark regression.** We used a ResNet50 as the backbone and the output of the forth convolutional block as the representation.

	MAFL	AFLW _M	AFLW _R	300W
w/o fine-tuning	2.73	8.83	7.37	6.01
w/ fine-tuning	2.81	7.80	6.99	5.94

B Visualization of feature embeddings

To better understand the information encoded in the learned representations, we visualize the first few PCA (uncentered) components in Fig. 4. Specifically, we sample hypercolumns from 32 MAFL images using our contrastively pretrained ResNet50, treat each spatial location separately and compute the PCA basis vectors. We then project the hypercolumns to each basis and visualize the projection as a spatial map. We observe that the first few PCA bases encode the background, foreground, and landmark regions (*e.g.* eyes, nose, mouth, etc.) of human faces. As a reference, we provide the PCA visualization of a random initialized ResNet50 with hypercolumn as representation.

C Memory efficiency

Tab. 5 compares the memory efficiency between DVE [46] and our model. To compute the equivariance loss, DVE needs to maintain high-resolution feature maps across the network hierarchy. By comparison, our contrastive learning loss is computed on a global image representation which requires less memory per-image during training.

Table 5: **Memory efficiency.** We compare the networks used by DVE [46] and our method in terms of number of network parameters (# Params), memory required for storing the network (Network Size), and the memory usage of a forward and backward pass on a single 96×96 image (Memory).

Method	Network	# Params (M)	Network Size (MB)	Memory (MB)
DVE [46]	Hourglass	12.61	48.10	491.85
Ours	ResNet18	11.24	42.89	11.54
	ResNet50	23.77	90.68	52.65

D Other implementation details

Training details of unsupervised learning models. We use MoCo [21] as our contrastive learning model. We train MoCo for 800 epochs with a batch size of 256 and the cosine learning rate schedule as proposed in [5]. However, we did not observe improvements in our task when using other tricks in [5], such as adding Gaussian blur for the data augmentation and using a MLP as the projection

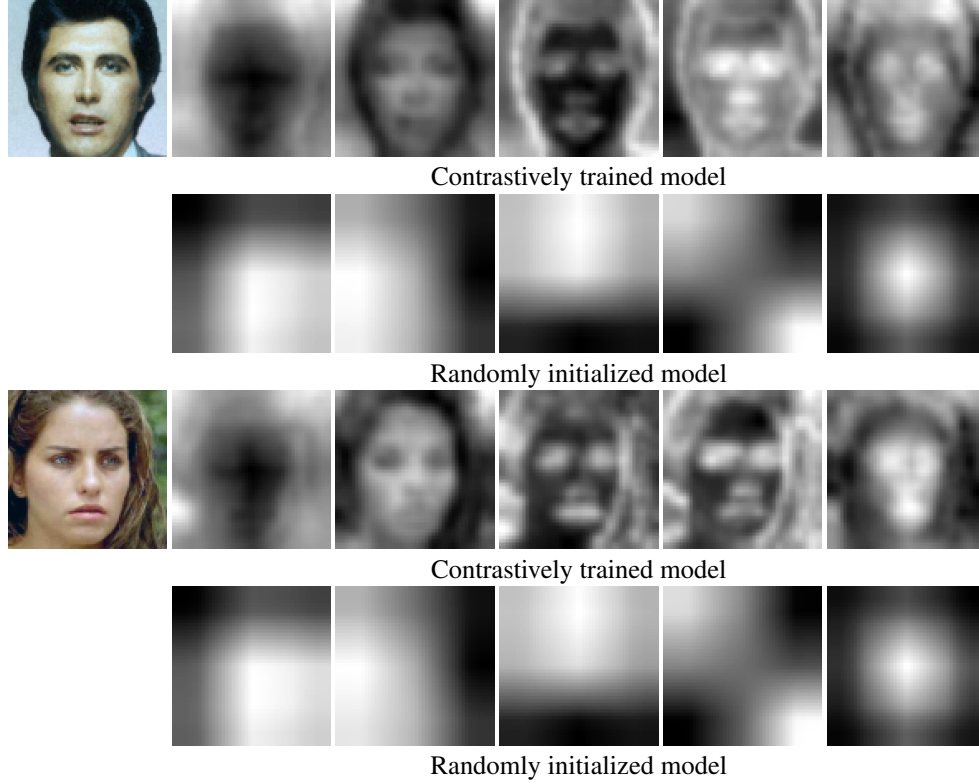


Figure 4: **PCA visualization of the hypercolumn representation.** From left to right: input image, and the projection of hypercolumns on the first five PCA bases. For each example we visualize the PCA components of a contrastively trained (top) and a randomly initialized ResNet50 (bottom).

network. We use the public implementation⁵ of MoCo from Tian et al. [47]. For a comparison with DVE model [46] on the proposed bird dataset, we use their publicly available implementation⁶.

Training details of linear regression. For the limited annotation experiments on human face benchmarks, we apply thin-plate spline as the data augmentation method with the same deformation hyperparameters as DVE [46]. We do not use any data augmentation for the experiments on the CUB dataset. To avoid excessive hyper-parameter tuning we train the linear regressor for 120, 45, and 80 epochs on MAFL, AFLW, and 300W dataset respectively, and keep them fixed for all ablation studies. On CUB, the results are reported from the checkpoint selected on the validation set. In the ablation study of the effectiveness of unsupervised learning (Tab. 3), for the ImageNet pretrained or randomly initialized networks, we report the best performance on the test set within 2000 training epochs. We use an initial learning rate of 0.01 and a weight decay of 0.05 when only limited annotations are available (Fig. 3a,b). The two hyperparameters are 0.001 and 0.0005 respectively when the entire annotations are given (Tab. 1). We use Adam [27] as the optimizer, and apply the cosine learning rate schedule.

E Birds benchmark

To test the performance of models on a challenging setting, we train representations in an unsupervised manner on iNaturalist Aves and evaluate on the CUB dataset. We randomly sample 100K images of birds from the iNaturalist 2017 dataset [50] under “Aves” class. Figure 5 top shows images from iNaturalist Aves dataset which contains birds in background clutter, occlusion, and with a wide range of pose variations and sizes than frontal faces in the human face benchmarks (*e.g.* MAFL). Some images even contain multiple birds. To test the performance in the few-shot setting, we sample

⁵<https://github.com/HobbitLong/CMC>

⁶<https://github.com/jamt9000/DVE>

a subset of CUB dataset which contains similar species to iNaturalist. Specifically we sample 35 species of *Passeroidea* superfamily, each annotated with 15 landmarks. We sample at most 60 images per class and conduct the splitting of training, validation and test set on the samples of each species in a ratio of 3:1:1. These splits are then combined, which results in 1241 training images, 382 validation images, and 383 testing images. Figure 5 bottom shows images from the CUB dataset, which are usually more object-centric and only have one bird per image.



Figure 5: **Images from bird datasets.** Images in CUB dataset (bottom) are iconic with birds more frequently in canonical poses and contain a single instance. On the other hand, iNaturalist images (top) are community driven and less curated. Often multiple birds are in a single image and are far away. This makes learning and transfer more challenging.

F Tables for Figure 3

Tab. 6, 7, and 8 present the numbers corresponding to Fig. 3a, b, and c respectively, which describe the effect of dataset size for landmark regression and unsupervised learning.

Table 6: **Landmark regression with limited annotations on AFLW_M benchmark.** The results are reported as percentage of the inter-ocular distance (lower is better).

Self-supervision	# of annotations					
	1	5	10	20	50	100 10122
None (SmallNet) [46]	28.87	32.85	22.31	21.13	–	– 14.25
DVE (Hourglass) [46]	14.23	12.04	12.25	11.46	12.76	11.88 7.53
	±1.54	±2.03	±2.42	±0.83	±0.53	± 0.16
Ours (ResNet50 + hypercol.)	42.69	25.74	17.61	13.35	10.67	9.24 6.99
	±5.10	±2.33	±0.75	±0.33	±0.35	± 0.35
Ours (ResNet50 + conv4)	43.74	21.25	16.51	12.45	10.03	9.95 8.05
	± 2.78	±1.14	±1.43	±0.66	±0.21	± 0.17
Ours (ResNet18 + hypercol.)	47.15	24.99	17.40	13.87	11.04	9.93 8.59
	± 6.88	±3.21	±0.37	±0.66	±0.92	±0.39
Ours (ResNet18 + conv4)	38.05	21.71	16.60	14.48	12.20	11.02 10.61
	±5.25	±1.57	±0.61	±0.69	±0.36	±0.06

Table 7: **Landmark regression on bird dataset.** The results are reported as the percentage of correct keypoints (PCK) metric (higher is better).

Self-supervision	# of annotation					
	10	50	100	250	500	1241
None (ResNet18)	2.97	10.07	11.31	24.82	38.86	52.64
DVE (Hourglass) [46]	37.82	51.64	54.58	56.78	58.64	61.91
Ours (ResNet18)	13.41	25.91	34.02	51.70	56.77	62.24
Ours (ResNet50)	13.87	29.28	40.86	57.96	64.55	68.63

Table 8: **The effect of training set size on unsupervised learning models.** The results are reported as percentage of the inter-ocular distance. The performance on MAFL and 300W are saturated given more than 50% unlabeled data. One possible reason is that MAFL and 300W provide many more annotations than AFLW. Notice that although 300W contains only 3148 training images, there are 68 annotations per image.

Dataset	Training set size					DVE [46]
	5%	10%	25%	50%	100%	
MAFL	3.87	3.29	3.09	2.43	2.44	2.86
AFLW _M	13.26	9.12	7.82	7.22	6.99	7.53
AFLW _R	11.47	8.69	7.71	6.61	6.27	6.54
300W	9.23	6.92	6.38	5.13	5.22	4.65